Potentiating Bisphosphonate-based Coordination Complexes to Treat Osteolytic Metastases

Journal:	*Journal of Materials Chemistry B*
Manuscript ID	TB-ART-08-2019-001857.R2
Article Type:	Paper
Date Submitted by the Author:	04-Feb-2020
Complete List of Authors:	Quiñones Vélez, Gabriel; University of Puerto Rico Rio Piedras, Department of Chemistry Carmona-Sarabia, Lesly; University of Puerto Rico Rio Piedras, Department of Chemistry Rodríguez-Silva, Waldemar; University of Puerto Rico Rio Piedras, Department of Biology Rivera Raíces, Alondra; University of Puerto Rico Rio Piedras Feliciano-Cruz, Lorraine; Universidad de Puerto Rico Recinto de Rio Piedras, Department of Biology Hu, Chunhua; New York University, Department of Chemistry Peterson, Esther; University of Puerto Rico Rio Piedras, Department of Biology Lopez-Mejias, Vilmali; University of Puerto Rico Rio Piedras, Department of Chemistry

SCHOLARONE™
Manuscripts

Potentiating Bisphosphonate-based Coordination Complexes to Treat Osteolytic Metastases

Gabriel Quiñones Vélez[a,b], Lesly Carmona-Sarabia[a,b], Waldemar A. Rodríguez-Silva[b,c],
Alondra A. Rivera Raíces[b,c], Lorraine Feliciano Cruz[b,c],
Tony Hu,[d] Esther Peterson,[c] and Vilmalí López-Mejías[a,b],*

[a] Department of Chemistry, University of Puerto Rico, Río Piedras
San Juan, Puerto Rico, 00931 United States.

[b] Crystallization Design Institute, Molecular Sciences Research Center,
University of Puerto Rico, San Juan, Puerto Rico,00926 United States.

[c] Department of Biology, University of Puerto Rico, Río Piedras
San Juan, Puerto Rico, 00931 United States.

[d] Department of Chemistry and the Molecular Design Institute,
New York University, 100 Washington Square East,
New York, New York 10003-6688, United States.

*vilmali.lopez@upr.edu

Abstract.
The hydrothermal reaction between bioactive metals (Ca^{2+}, Zn^{2+}, and Mg^{2+}) salts and clinically utilized bisphosphonate, alendronate (ALEN), promotes the formation of several materials denominated as bisphosphonate-based coordination complexes (BPCCs). The systematic exploration of the effect of three variables M^{2+}/ALEN molar ratio, temperature, and pH on the reaction yielded an unprecedented number of materials of enough crystal quality for structural elucidation. Five crystal structures were unveiled by X-ray diffraction (ALEN-Ca forms I and II, ALEN-Zn forms I and II, and ALEN-Mg) and their solid-state properties revealed in tandem with other techniques. The dissolution of these BPCCs was tested and contrasted to that of the commercially employed generic form of *Fosamax®* Alendronate Sodium, using fasted-state simulated gastric fluid and phosphate-buffered saline solution. Quantification of ALEN content was performed by derivatization with Cu^{2+}, which produced a soluble complex suitable for quantification. Results show that these materials present a pH-dependent degradation. Moreover, a phase inversion temperature (PIT) nano-emulsion method was applied to the synthesis of ALEN-Ca form II. Size distribution analysis demonstrated the efficiency of the PIT-nano-emulsion method to decrease the particle size of this BPCC from ~60 μm to ~438 d.nm. The cytotoxicity of ALEN, ALEN-Ca form II (bulk crystals), and nano-Ca@ALEN (nanocrystals) against the MDA-MB-231 cell line was investigated. Nano-Ca@ALEN form II presents higher cytotoxicity effects than ALEN and ALEN-Ca form II (bulk crystals), showing inhibition of cell proliferation at 7.5 μM. These results provide evidence of the structure, stability, dissolution and cytotoxicity properties of ALEN-based BPCCs and pave the way for better formulation strategies for this drug through the design of nano-sized BPCCs for the treatment of bone-related diseases.

Introduction.

Over 18.1 M new cancer cases and 9.6 M cancer deaths occurred worldwide in 2018.[1] Cancer can spread to any part of the body, though certain types spread preferentially. Patients with breast, prostate and lung cancer are more prone to develop bone metastases.[2] Of the total annual cases of breast cancer, the majority are invasive with high potential for metastases.[3] The resulting carcinomas are highly heterogeneous and distinct subtypes have been identified based on histopathology, putative cell of origin, genetic profiling and clinical outcomes. Estrogen receptor alpha positive (ER+) and progesterone receptor positive (PR+) breast cancers account for 60-70% of the breast cancers diagnosed in humans.[3] While less common, basal-like tumors which are triple-negative (ER-, PR-, HER2-) are generally more aggressive and tend to metastasize.[3]

About 70% of patients with metastatic breast cancer develop osteolytic metastases (OM) over the course of their disease leading to severe bone pain, fractures, hypercalcaemia and nerve compression syndrome.[2,4] Breast and lung cancers lead mainly to bone osteolytic lesions characterized by bone destruction that results from enhanced osteoclast activity, altering bone remodeling at the bone marrow.[2] Tumor cells that metastasize to the bone marrow use bone-derived growth factors involved in the coupling between osteoclasts and osteoblasts to promote their own development. Osteoclast mediated bone resorption plays a critical role in the progression of metastatic bone disease; hence, osteoclasts are prominent therapeutic targets for bone metastases.

Although lung and prostate cancers are statistically relevant, this study focuses on the development of pharmaceutical coordination complexes geared towards the treatment and prevention of breast-cancer-induced bone metastases as it affects men, women and the elderly. Models for metastatic disease includes the MDA-MB-231 cell line, which is ER, PR and E-cadherin negative, and expresses mutated p53.[3] MDA-MB-231 microarray profiling matches with the basal subtype of breast cancer, and since the cells also lack growth factor receptor HER2, they represent a good model of triple-negative breast cancer.[3] In this work, MDA-MB-231 cell line was chosen as a model to study breast-cancer-induced OM, as it present specific micro-RNAs that are involved in the metastatic cascade that lead to bone metastasis formation.[2]

Bisphosphonates (BPs), a general group of bone-resorption inhibitors, are commonly prescribed to treat OM and for the management of breast-cancer-induced bone metastases.[5,6,7] BPs are characterized by the presence of P-C-P bonds, which resist enzymatic hydrolysis, in contrast to pyrophosphates (P-O-P bonds).[7,8] These compounds exhibit high affinity to calcium ions, thus, BPs present strong binding to bone.[9] There is accumulating evidence that BPs induce tumor-cell apoptosis contributing to the decrease in tumor burden at the metastatic site.[5,10,11,12] BPs have demonstrated anti-tumor effects via direct (tumor cell adhesion and invasion, apoptosis) and indirect (angiogenesis, γδ T cells) mechanisms in preclinical research.[13] However, their direct anti-tumor effect remains inconsistent in *in vivo* clinical research.[14] This might be due to the high doses required to achieve clinically meaningful anti-tumor effects.[14] BPs suffer from pharmacological deficiencies such as poor bioavailability and intestinal adsorption (<10%), leading to low blood plasma concentrations.[6,12,15,16] What does get absorbed is distributed to the bone (40-60% of the dose) and the excess is excreted in the urine.[12,15,16]

Metal complexes containing bioactive ligands provide new avenues for drug development were the release of the biomolecule is achieved through the degradation of the structure under biological conditions. When compared to polymeric drug delivery systems, coordination complexes (CCs) present well-defined crystalline structures, properties and stability, which can facilitate characterization and decrease result variability. Already metal ions such as Ni^{2+}, Cu^{2+}, Co^{2+}, Cd^{2+}, Mn^{3+}, Cr^{3+}, Mo^{6+}, Li^+ have been used to coordinate with BPs to form

CCs.[17,18,19,20,21,22,23,24,25] Yet, the biocompatibility of these metals used to construct CCs containing BPs remains a concern, hindering their success in biomedical applications.

In this work, alendronate (ALEN, **Figure 1**), a second-generation BP used for the treatment of osteoporosis, Paget's disease and hypercalcemia, is employed for its coordination with bioactive metals to form a series of CCs denominated as bisphosphonate-based coordination complexes (BPCCs). BPs are ideal ligands for constructing BPCCs because these (1) possess multiple binding modes, which pave the way for a variety of structures able to reach the targeted site through uncoordinated BPs at the BPCC surface, (2) present low cytotoxicity, and (3) do not significantly metabolize. In terms of the metal, three bioactive metals ($M^{2+} = Ca^{2+}$, Zn^{2+} and Mg^{2+}), with LD_{50} of 0.35, 1.0 and 8.1 g/kg, respectively, were chosen because for their essential roles in promoting osteoblastic bone formation and mineralization.[26,27,28]
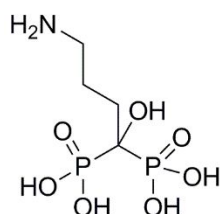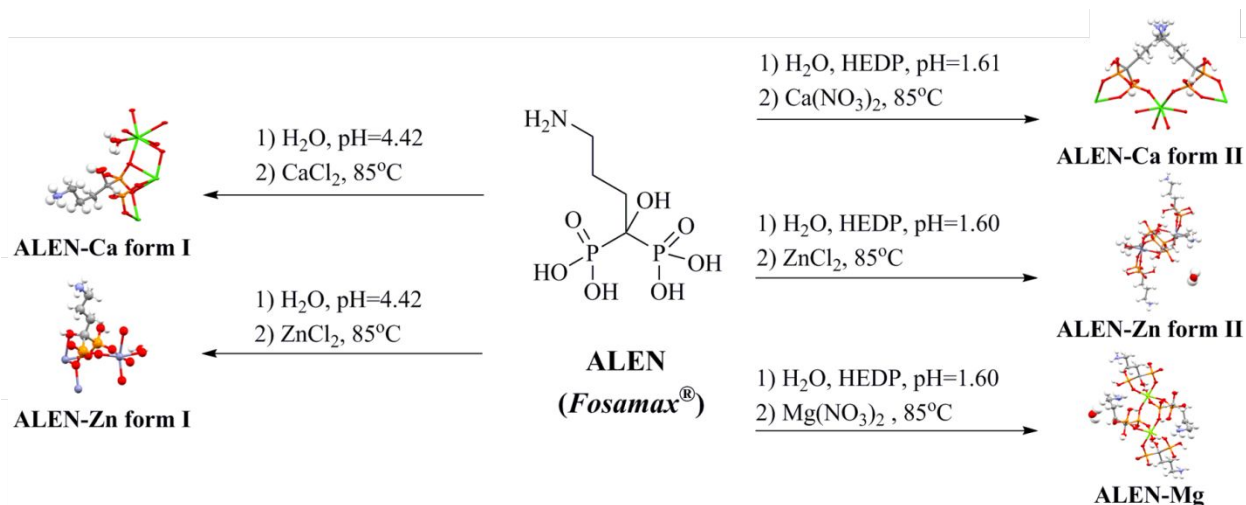

ALEN

(*Fosamax*®)

Figure 1. Molecular structure of alendronic acid (ALEN), a bisphosphonate (BP) with clinical relevance, utilized in the design of bisphosphonate-based coordination complexes (BPCCs).

This study is intended to address the shortcomings of currently known ALEN-based CCs in terms of particle size and cytotoxicity of the metal cluster required for drug delivery applications.[17,18,19,20,22,23] The systematic exploration of the effect of three variables M^{2+}/ALEN molar ratio, temperature, and pH on the reaction outcomes yielded an unprecedented number of crystalline materials of enough crystal quality for structural elucidation. For five of these materials (**Figure 2**), the crystal structure was unveiled by single crystal X-ray diffraction and their solid-state properties revealed in tandem with other characterization techniques. In this work, we employ a phase inversion temperature (PIT)-nano-emulsion method to confine the reaction of ALEN with biocompatible metals into the nano-range, limit crystal nucleation and reduce crystal size. Ultimately, studies addressing structural stability under physiological conditions and cytotoxicity of the ALEN-based BPCCs may lead to expand and integrate molecular design principles for nano-BPCCs and to apply these to unveil the biomedical applications of these materials in the treatment and prevention of OM; a disease that affects a significant portion of cancer patients.

Figure 2. Schematic diagram of the design space explored leading to five crystalline phases when alendronate (ALEN) coordinated with three bioactive metals (Ca^{2+}, Zn^{2+}, and Mg^{2+}) and in some cases an auxiliary ligand, etidronate (HEDP). The variables explored were; M^{2+}/ALEN molar ratio, reaction temperature, and pH.

Experimental section.

Materials: Calcium nitrate tetrahydrate [Ca(NO$_3$)$_2$·4H$_2$O, 99% pure], calcium chloride hexahydrate [CaCl$_2$·6H$_2$O, USP grade], zinc nitrate hexahydrate [Zn(NO$_3$)$_2$·6H$_2$O, 98% pure], zinc chloride anhydrous [ZnCl$_2$, >98%], magnesium nitrate hexahydrate [Mg(NO$_3$)$_2$·6H$_2$O, 99% pure], and etidronic acid 60% aqueous solution (HEDP) were purchased from Sigma-Aldrich (St. Louis, MO). Alendronate sodium trihydrate (ALEN), 97% pure was purchased from TCI America (St. Portland, OR). A stock solution of sodium hydroxide (NaOH, USP grade, 1.5 M) was used for pH adjustments. Distilled water was used as solvent in all syntheses.

MDA-MB-231 (ATCC® HTB-26™, Manassas, VA) cell line, fetal bovine serum (FBS), and penicillin-streptomycin (Pen-Strip) were purchased from Sigma-Aldrich (St. Louis, MO), whereas Dulbecco's Modified Eagle's Medium (DMEM) was purchased from Sigma-Aldrich (Milwaukee, WI). AlamarBlue® was purchased from Bio-Rad (Kidlington, Oxford) and used to determine cell proliferation.

General hydrothermal synthesis for ALEN-based BPCCs. The hydrothermal synthesis of ALEN-based BPCCs was performed by preparing ALEN solutions and the metal salt separately in distilled water at room temperature. If required, the pH of the ligand solution was adjusted with 1.5 M NaOH above several of the pK$_a$'s of the ligand (pH = 1.61 – 4.42), where a partially deprotonated phosphonate is the main species present in solution. In some instances, HEDP was added as an auxiliary ligand to decrease the pH below of the pK$_a$'s of the principal ligand (ALEN). Using a syringe, the metal salt solution was added drop wise to the ligand solution and mixed thoroughly. The pH of the resulting solution was adjusted below the pH leading to the formation of the metal hydroxide. The resulting mixture was heated until crystals appeared, here, the nucleation induction times varied between minutes to hours. After the crystals were visually detected, the vials were removed from heat and left undisturbed to aid the growth of the crystals. The product was collected by vacuum filtration and air-dried. Detailed information for the conditions leading to each of the BPCC (ALEN-Ca forms I and II, ALEN-Zn forms I and II, and ALEN-Mg) presented is available in the *Supporting Information.*

Raman microscopy. Raman spectra were recorded in a Thermo Scientific DXR Raman

microscope, equipped with a 532 nm laser, 400 lines/nm grating, and 50 μm slit. The spectra were collected at room temperature over the range of 3,400 and 100 cm^{-1} by averaging 32 scans with exposures of 5 sec. The OMNIC for Dispersive Raman software version 9.2.0 was employed for data collection and analysis.

Scanning electron microscopy-energy dispersive spectroscopy (SEM-EDS). Micrographs and X-ray microanalysis were recorded with a JEOL JSM-6480LV scanning electron microscope with an Evenhart Thomley secondary electron imagining (SEI) detector and an energy dispersive X-ray analysis (EDAX) Genesis 2000 detector. Images were taken with an acceleration voltage of 20 kV, an electron beam of 11 mm width, with a spot size value of 36, SEI signal and high vacuum mode.

Powder X-ray diffraction (PXRD). Powder diffractograms were collected in transmission mode (100 K) using a Rigaku XtaLAB SuperNova X-ray diffractometer with a micro-focus Cu-Kα radiation (λ = 1.5417 Å) source and equipped with a HyPix3000 X-ray detector (50 kV, 1 mA). Powder samples were mounted in MiTeGen micro loops. Powder diffractograms were collected between 6 − 60° with a step of 0.01^o using the Gandalfi move experiment. Data was analyzed within the CrystAllis^{PRO} software v. 1.171.3920a.

Single crystal X-ray diffraction (SCXRD). The crystals were observed under the microscope using polarized light to assess their quality. Optical micrographs were recorded with a Nikon Eclipse Microscope LV100NPOL, equipped with a Nikon DS-Fi2 camera and NIS Elements BR software version 4.30.01. Suitable single crystals were mounted in MiTeGen micro loops for structure elucidation. Structural elucidation was performed in either of two instruments; crystal structure for ALEN-Zn form I was collected in a Bruker AXS SMART APEX-II single crystal diffractometer equipped with a Monocap collimator and APEX-II CCD detector with a Mo-Kα (λ = 0.71073 Å) radiation source operating at 50 kV and 40 mA. The data collection was carried out at 100 K using an Oxford Cryosystems Cryostream 700 cooler.

Other crystal structures (ALEN-Ca forms I and II, ALEN-Zn form II and ALEN-Mg) were collected with a Rigaku XtaLAB SuperNova single micro-focus Cu-Kα radiation (λ = 1.5417 Å) source equipped with a HyPix3000 X-ray detector in transmission mode operating at 50 kV and 1 mA within the CrystAllis^{PRO} software v. 1.171.3920a. The data collection was carried out at 100 K using an Oxford Cryosystems Cryostream 800 cooler. All crystal structures were solved by direct methods. The refinement was performed using full-matrix least squares on F^2 within the Olex2 software v1.2. All non-hydrogen atoms were anisotropically refined.

Thermogravimetric analysis (TGA). TGA of ALEN and the ALEN-based BPCCs were recorded in a Q500 (TA Instruments Inc.) between 30 − 700°C at 5 °C/min under a N$_2$ gas purge (60 mL/min). In all cases, ~10 mg of powder sample was thermally treated. Data was analyzed with TA Universal Analysis software version 4.3A.

Dissolution rate measurements. Dissolution profiles were performed via complexation of ALEN with Cu (II) and quantified by measuring absorbance through UV-Vis spectroscopy. Dissolution profiles were recorded for ALEN sodium reagent, ALEN Sodium Tablets-USP (generic form of Fosamax®), ALEN-Ca forms I and II, and ALEN-Zn forms I and II, and ALEN-Mg. Dissolution tests were performed in 100 mL of PBS buffer (pH = 7.40) and FaSSGF (pH = 1.60), at 37°C under constant stirring at 150 rpm. The absorbance of the soluble ALEN-Cu complex was measured at 231 nm in PBS and 225 nm in FaSSGF, against a reagent blank. Absorbance measurements were performed on an Agilent Technologies Cary Series UV-Vis Spectrophotometer, Cary 100 UV-Vis model; using the UV Cary Scan software version v.20.0.470. All measurements were performed with a 400-200 nm scan.

Determination of the phase inversion temperature (PIT) and PIT-nano-emulsion synthesis

of nano-Ca@ALEN form II. To reduce the particle size, a PIT-nano-emulsion method was employed during the synthesis of a selected BPCC, specifically ALEN-Ca form II. The PIT temperature was determined by measuring the conductivity of an aqueous emulsion containing ALEN in heptane (oil phase) and Brij L4® (surfactant) during a temperature profile (2-60°C at 1°C/min). After homogenizing the emulsions, conductivity measurements started at 2°C with an O/W micro-emulsion. As the emulsion is heated, a phase inversion occurs from oil in water (O/W, conductive) micro-emulsion to water in oil (W/O, not conductive) nano-emulsion.

The nano-emulsion synthesis of nano-Ca@ALEN form II was conducted in a Crystalline (Technobis, Crystallization Systems, Alkmaar, Netherlands). The pre-homogenized emulsions (ALEN, heptane, Brij L4®) prepared for the PIT determination were used to perform the nano-Ca@ALEN form II nano-emulsion synthesis. The emulsion was homogenized before being transferred to the reaction vial and placed in the first reactor at a temperature 7°C and 1,250 rpm for 30 min. After the 30 min elapsed, the reaction vial was transferred to a second reactor at 45°C and 1,250 rpm. The emulsion was stirred for 30 min before heating to the reaction temperature 85°C. Subsequently, the metal salt solution was added with a syringe and left undisturbed for 30 min. Once completed, the reaction vial was left undisturbed for 1 h before analyzing the supernatant from the aqueous phase using dynamic light scattering (DLS).

Samples resulting from the nano-emulsion synthesis of nano-Ca@ALEN form II were analyzed in a Malvern Panalytical Zetasizer NanoZS equipped with a He-Ne orange laser (633nm, max 4 mW) (Spectris PLC, Surrey, England). Data was analyzed with Malvern software version 7.12. Aliquots of 50 μL of the supernatant from the aqueous phase were transferred to disposable polystyrol/polystyrene cuvettes (REF: 67.754 10 x 10 x 45 mm) (Sarsted, Germany), in a 1:20 dilution ratio with nanopure water. The refractive index of ALEN in water is 1.334. This value was determined by measuring an aliquot of ALEN stock solution with a Mettler Toledo Refracto 30GS (Mettler Toledo, Columbus, OH).

Cell culture conditions. MDA-MB-231 were maintained in DMEM supplemented with 10% FBS and 1.0 % of Pen-Strep. Cells were cultured at 37°C in a humidified atmosphere of 5.0 % CO_2 and harvested from sub confluent (< 80%) cultures using a 0.05% trypsin-EDTA solution.

Cytotoxicity assay. Cell viability was determined with a resazurin-based assay (AlamarBlue®). MDA-MB-231 cells were seeded (2.5×10^4 cell/well) in DMEM with 10% FBS in a 96-well plate. After 24 h, cells were treated with 2-fold serial dilutions (0-145 μM) of ALEN, ALEN-Ca form II (bulk crystals) or nano-Ca@ALEN form II (nanocrystals), and incubated for 24, 48 and 72 h. The medium was then fully replaced with fresh serum-free DMEM containing 10% AlamarBlue®. The cells were incubated for 4 h at 37°C, and fluorescence signal (λ_{exc} = 570 nm, λ_{em} = 590 nm) was measured in an Infinite M200 PRO Tecan Microplate Reader. After baseline correction, the measured signal was normalized to the non-treated cells designated to be 100% viable. Nonlinear regression in Graph Pad Prism 8 was utilized to fit the growth curve over the various drug concentrations to determine the half-maximal inhibitory concentration (IC_{50}).

Concentration of 7.5, 15 and 30 μM of ALEN, ALEN-Ca form II (bulk crystals), and nano-Ca@ALEN form II (nanocrystals) were prepared and used to determine the percentage of cell viability (% RCV) after 24, 48 and 72 h. Graph Pad Prism 8 was employed to plot the % RCV in the different concentrations and time points. All data was statistically treated taking in consideration mean, standard deviation, and coefficient of variation percentage (%CV).

Results and Discussion.

The majority of the successful ALEN-based BPCCs formed while employing a 1:1 M^{2+}/ALEN molar ratio at 85 °C, and in acidic media (pH < 7.0). Many of the hydrothermal synthesis spontaneously formed microcrystalline powders, interestingly; in most of these cases Mg^{2+} was employed as the bioactive metal. A schematic diagram for the syntheses of selected ALEN-based BPCCs is presented in **Figure 2**. In some cases, an auxiliary ligand, etidronate (HEDP) was added to the hydrothermal reaction to promote the formation of high quality single crystals. Five ALEN-based BPCCs were produced as single crystals with enough quality for structural elucidation by single X-ray diffraction (**Figure 3**). For these coordination complexes, their solid-state, stability in physiological media, particle size and cytotoxicity were assessed and/or optimized to potentiate their biomedical applications in the treatment and prevention of OM.
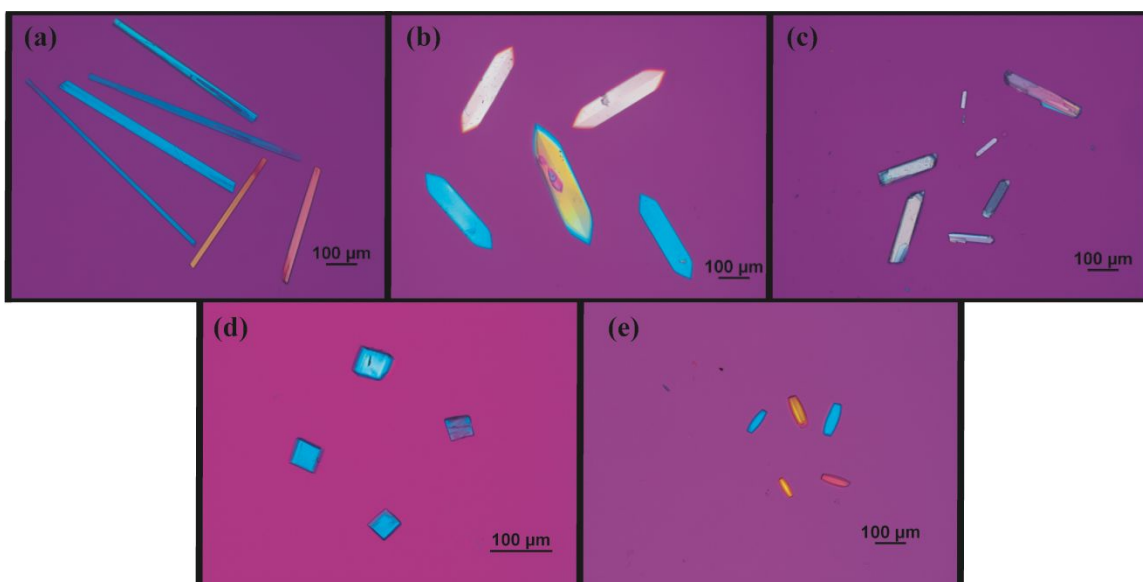

Figure 3. Polarized optical micrographs of ALEN-based BPCCs presenting the highest quality single crystals; (a) ALEN-Ca form I, (b) ALEN-Ca form II, (c) ALEN-Zn form I, (d) ALEN-Zn form II, and (e) ALEN-Mg.

Raman spectroscopy analysis.

Representative Raman spectra for the isolated ALEN-based BPCCs were collected between 3,400 and 100 cm^{-1}, and are shown in **Figure 4**. The presence and absence of characteristic Raman shifts in the spectra of ALEN and the ALEN-based BPCCs indicates that a distinctive solid-form had been produced (Supporting Information). Moreover, among the five phases, significant differences are observed. These differences occurred particularly in the 2,650 – 2,800 cm^{-1} region, where characteristic bands can be assigned to the presence of hydrogen phosphate, H–OPO_2C moieties.[29] Raman shifts between 3,200 – 3,600 cm^{-1} are assigned to the νO–H/H_2O stretching vibrations of different moieties: hydroxyl groups in ALEN, coordinated and lattice water molecules (**Figure 4**).[29] These suggest that extensive hydrogen bonding might be present in the ALEN-based BPCCs. The broadening and splitting of these bands indicate the presence of several types of strong hydrogen bonds (~ 3200 cm^{-1}) within each lattice. The presence of ALEN in the molecular structure of the product is confirmed by two bands at 1,100 cm^{-1} (medium) and 1,046 cm^{-1} (strong), respectively, which are characteristic bands for both the ν^{as}P-O(H) asymmetric stretching vibrations and the δPO-H bending of the phosphonate P–O_3

groups.[29,30,31] The band at around $1{,}140 - 1{,}160$ cm^{-1} is characteristic of νP=O/δ^{π}POH stretching vibrations.[29,30] The band at $1{,}260$ cm^{-1} may be attributed to the P=O deformation vibration. Similarly, to the asymmetric stretching vibration of the P-O bonds, Raman shifts between $930 - 1{,}000$ cm^{-1} correspond to the symmetric ν^{s}P-O(H) stretching vibrations.[29,30,31] Different vibrational modes of coordination of the divalent metal ions (M^{2+}) with phosphorus bonded oxygen atoms, induce changes in the P-O bond order, generating the differences observed in the symmetric and asymmetric P-O(H) stretching vibrations among the BPCCs and the ligand.[29] Other bands located at lower wavenumbers ($< 1{,}000$ cm^{-1}) correspond to vibrational modes characteristics of the CH$_2$, C–C, C-P, C-OH and M–O groups and are also present in the Raman spectra of the isolated ALEN-based BPCCs.[29]
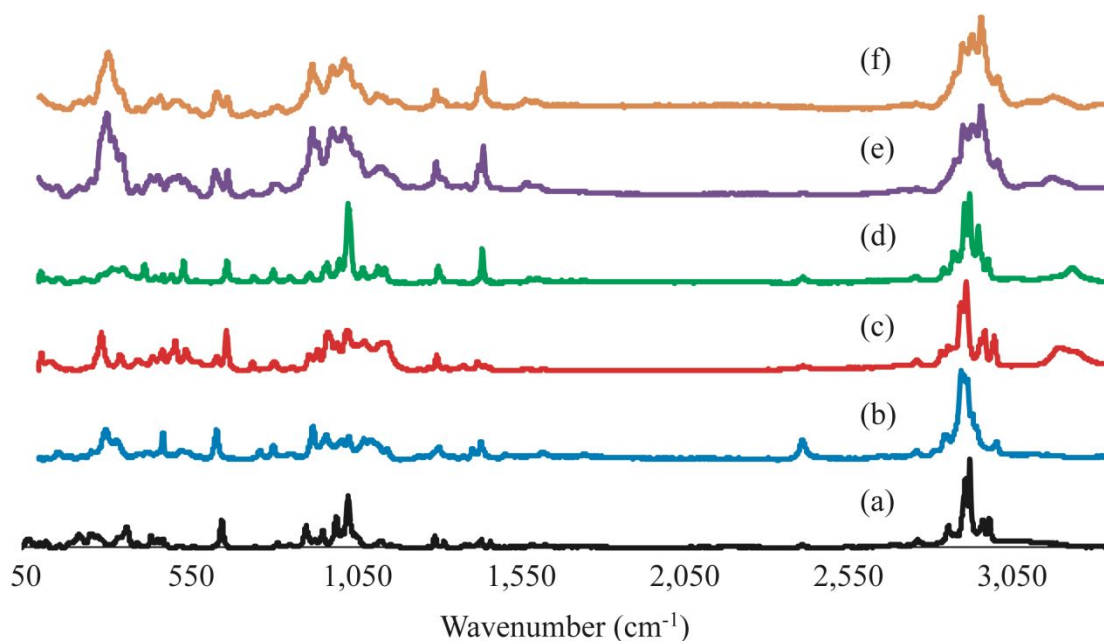
Figure 4. Raman spectra overlay of (a) alendronate (ALEN) and ALEN-based BPCCs; (b) ALEN-Ca form I, (c) ALEN-Ca form II, (d) ALEN-Zn form I, (e) ALEN-Zn form II, and (f) ALEN-Mg.

Scanning electron microscopy-energy dispersive X-ray spectroscopy (SEM-EDS).
To assess the morphology and basic composition of the yielded crystalline materials, analysis with SEM-EDS was performed. Representative SEM images collected for the isolated crystalline phases show crystals with well-defined morphologies (**Figure 5**). SEM images indicate that the diameter of the resulting crystals range between $40 - 200$ μm.
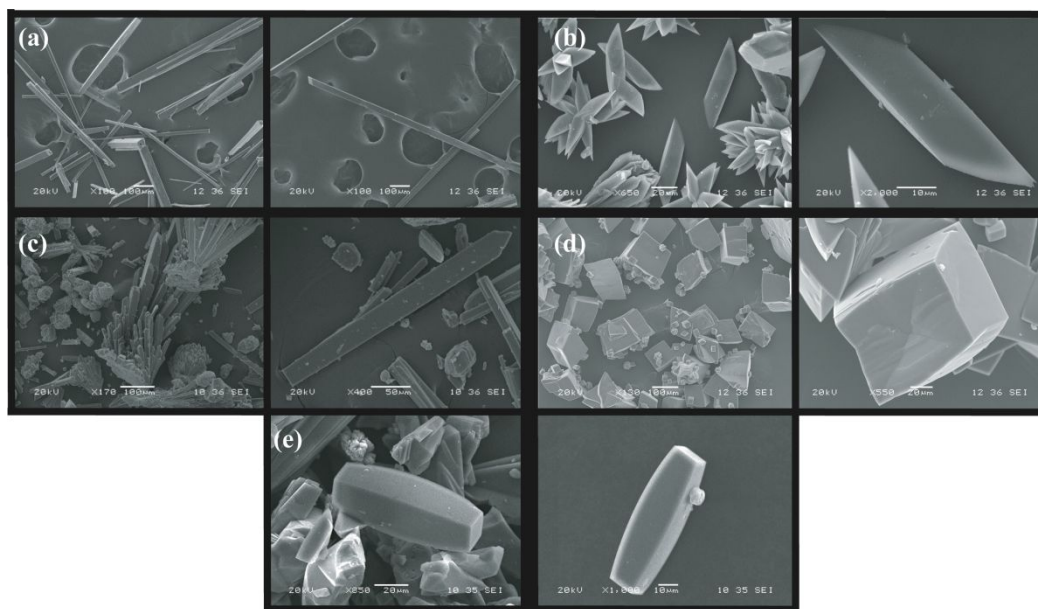
Figure 5. Representative scanning electron micrographs for the ALEN-based BPCCs; (a) ALEN-Ca form I, (b) ALEN-Ca form II, (c) ALEN-Zn form I, (d) ALEN-Zn form II, and (e) ALEN-Mg.

The EDS spectra of these materials exhibit the characteristic signals of the metal and other elements, which are present in the molecular structure of ALEN (carbon, nitrogen, phosphorous, and oxygen atoms), and had been employed in the hydrothermal reactions (**Figure 6**). These results along with the Raman spectra analysis support, thus far, that the hydrothermal reactions have produced five crystalline phases that are distinct from the starting materials employed.
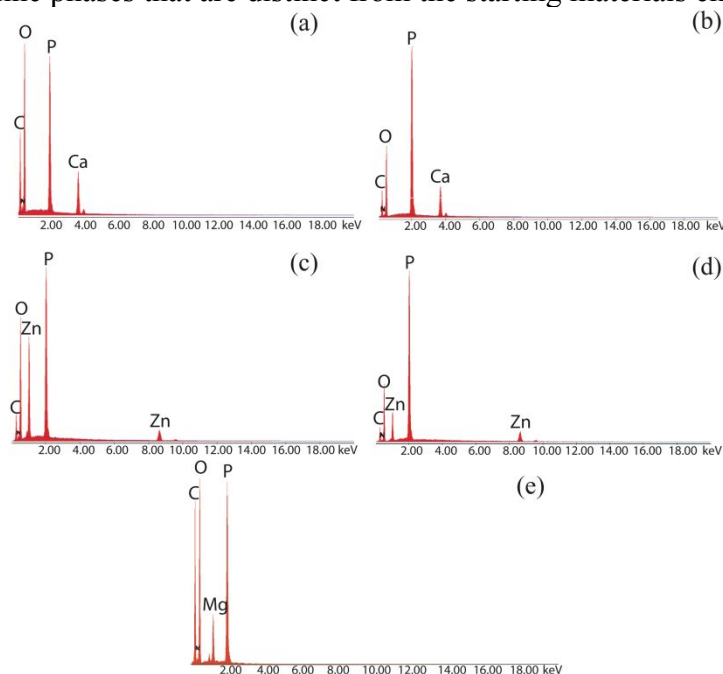

Figure 6. Representative energy dispersive spectra for the ALEN-based BPCCs; (a) ALEN-Ca form I, (b) ALEN-Ca form II, (c) ALEN-Zn form I, (d) ALEN-Zn form II, and (e) ALEN-Mg.

Powder X-ray diffraction (PXRD) analysis.

To assess the crystallinity of the products for the hydrothermal syntheses between ALEN (**Figure 1**) and bioactive metals (Ca^{2+}, Zn^{2+}, and Mg^{2+}), PXRD was performed. Here, we focus on the PXRD of five phases that presented the highest crystal quality as suggested by polarized optical microscopy (**Figure 3**). The observation of low amorphous background in each of the diffractograms of the isolated phases confirms a high degree of crystallinity (**Figure 7**). Moreover, PXRD analysis was utilized to confirm that these phases were not produced by the concomitant recrystallization of the metal salt or ALEN employed in each of the hydrothermal reactions (Supporting Information). Based on the differences in the diffractograms when the starting materials and the products of the hydrothermal syntheses were compared, the formation of distinctive crystalline phases can be sustained. The absence of low angle peaks (< 5 ° in *2θ*) suggests that these are dense or *2D* layered materials and not *3D* porous networks.

Previously reported crystal structures of ALEN-based CCs have been also examined and compared to those reported here.[17,18,19,23-25,32,33] ALEN-based BPCCs comprised of ALEN and calcium are structurally distinct from any other previously reported phases as demonstrated by the overlay of their respective diffractograms (Supporting Information).[32,33] ALEN-Zn form I is isostructural to two reported structures formed by the same ligand with either manganese or cobalt (Supporting Information).[23] ALEN-Zn form II and ALEN-Mg are isostructural to ALEN-Co, ALEN-Cu and ALEN-Ni structures previously reported.[19,24,25]
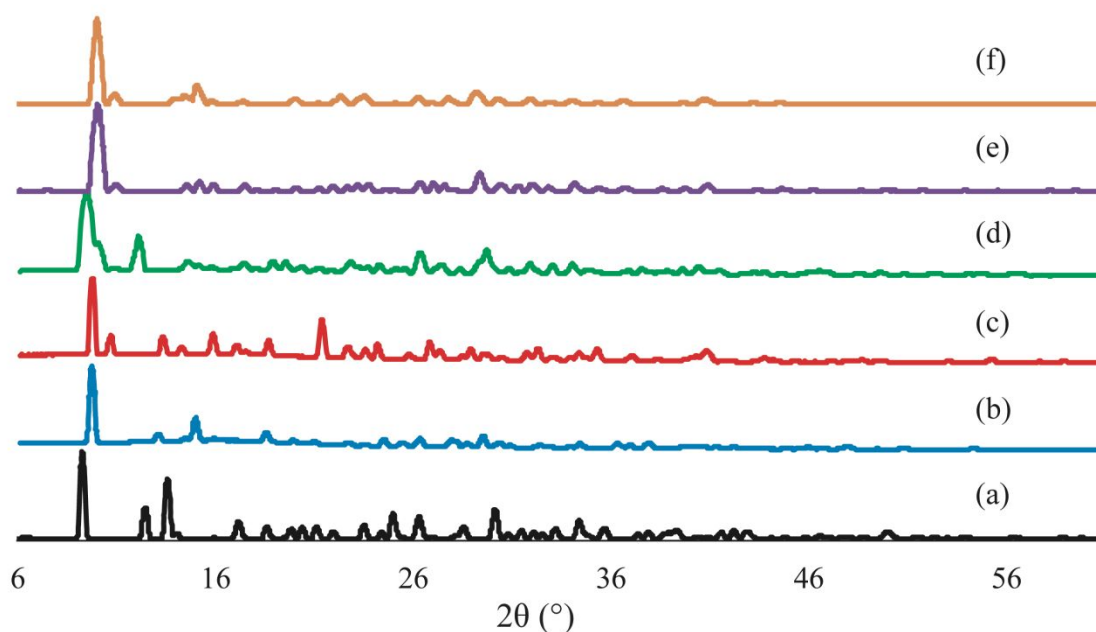
Figure 7. PXRD overlay of (a) alendronate (ALEN) and the ALEN-based BPCCs; (b) ALEN-Ca form I, (c) ALEN-Ca form II, (d) ALEN-Zn form I, (e) ALEN-Zn form II, and (f) ALEN-Mg.

Single crystal X-ray diffraction (SCXRD) analysis.

To provide unambiguous evidence for the formation of these five ALEN-based BPCCs, elucidation of their crystal structure was performed using SCXRD. The crystal structures were

collected at low temperature (100 K) and solved using direct methods. Summary of the crystallographic parameters of the structure refinements of each crystalline phase analyzed are summarized in **Table 1**. Further details can be found in the Supporting Information. PXRD overlays of the calculated powder patterns against the experimental powder patterns (Supporting Information) for each crystalline phase corroborates that a representative solution has been found, and that these were obtained as pure phases. To our surprise, for all hydrothermal reactions in which HEDP was employed as an auxiliary ligand (ALEN-Ca form II, ALEN-Zn form II and ALEN-Mg), the resulting phases did not incorporate the ligand in their crystalline lattice.

Table 1. Summary of the crystallographic parameters of the structure refinements of the isolated ALEN-based BPCCs; (a) ALEN-Ca form I, (b) ALEN-Ca form II, (c) ALEN-Zn form I, (d) ALEN-Zn form II, and (e) ALEN-Mg.

Compound	ALEN-Ca form I	ALEN-Ca form II	ALEN-Zn form I	ALEN-Zn form II	ALEN-Mg
Empirical formula	$Ca(C_4H_{13}NO_8P_2)$	$Ca(C_8H_{24}NO_{14}P_4)$	$[Zn(C_4H_{11}NO_7P_2)(H_2O)]$	$[Zn_2(C_{16}H_{48}N_4O_{28}P_8)$ $(H_2O)_2]\cdot 2H_2O$	$[Mg_2(C_{16}H_{46}N_4O_{28}P_8)$ $(H_2O)_2]\cdot 2H_2O$
FW (g/mol)	305.17	536.25	330.46	1195.14	1111.01
Space group	$Pna2_1$	$I\,2/a$	$P\,2_1/n$	$P\,2_1/n$	$P\,2_1/c$
Temperature (K)	100.15	100.01 (10)	100 (2)	100.00 (10)	100.00 (10)
λ (Å)	1.54184	1.54184	0.71073	1.54184	1.54184
a (Å)	13.5226 (2)	11.40590 (10)	5.4734 (7)	12.5428 (12)	12.5554 (2)
b (Å)	12.1976 (2)	12.38480 (10)	14.7092 (18)	13.4307 (2)	13.3948 (2)
c (Å)	6.75490 (10)	13.46860 (10)	12.2579 (15)	20.3723 (19)	12.4249 (2)
α (°)	90	90	90	90	90
β (°)	90	101.3320 (10)	98.003 (2)	144.93 (2)	109.283 (2)
γ (°)	90	90	90	90	90
V (Å^3)	1114.18 (3)	1865.48 (3)	977.3 (2)	1971.9 (6)	1972.36 (6)
Z	4	4	4	2	2
ρ_{calc} (g/cm^3)	1.819	1.909	2.246	2.013	1.871
Rwp	0.1164	0.0861	0.0832	0.1559	0.1997
Rp	0.0422	0.0331	0.0381	0.0590	0.0703

Abbreviations: λ (X-ray source wavelength, Å), a/b/c (unit cell lengths, Å), $\alpha/\beta/\gamma$ (unit cell angle, °), V (unit cell volume, Å^3), Z (number of formula units per unit cell), ρ_{calc} (unit cell calculated density, g/cm^3), R_{wp} (weighted R-factor, %), and R_p (R-factor, %).

Structural description of ALEN-Ca form I, In the compound $Ca(C_4H_{13}NO_8P_2)$, ALEN coordinates to the calcium atom through four unique metal oxygen bonds; two in the equatorial positions (Ca1–O1 = 2.292 Å and Ca1–O3 = 2.565 Å) and two in the axial positions of the octahedra (Ca1–O5 = 2.377 Å and Ca1–O6 = 2.337 Å). A disordered water molecule coordinates to the metal center (Ca1–O8 = 2.379 Å) completing the octahedra. Even though the water molecule acts as a terminal ligand, the ALEN ligand act as pillars linking neighboring calcium atoms forming a *3D* framework containing *1D* inorganic chains that stacked tilted along the *c*-axis. A single intramolecular hydrogen bond between oxygen of the ligand and the terminal water molecule (O2···O8 = 2.946 Å) reinforces the propagation of the *1D* chains motif. Adjacent chains

are bound by a series of intermolecular hydrogen bonds; along *b*-axis by the amine nitrogen of one ALEN and the oxygen atom of another ALEN ligand (O2···N1 = 3.020 Å) and along the *a*-axis several intermolecular hydrogen bonds (O5···N1 = 2.839 Å and O6···N1 = 2.845 Å, O2···O7 = 2.464 Å, O7···O8 = 2.670 Å). The hydrogen bond network helps to expend the *3D* framework along the *ab*-plane. This crystal structure is unique from those previously reported.[32,33]

Structural description of ALEN-Ca form II, The compound $Ca(C_8H_{24}NO_{14}P_4)$ crystallizes in the *I*2/a space group with the asymmetric unit containing a single independent calcium atom. The calcium atom has a strongly distorted octahedral environment with the O–Ca–O bond angles ranging from 79.79 º to 105.30 º. The Ca–O bond distances range between 2.287 Å and 2.343 Å. The calcium atom is coordinated by two symmetry related ALEN ligands. No coordinated water or lattices waters are present in this structure unlike the previous structure solved for ALEN-Ca form I. The ALEN ligands act as pillars linking neighboring calcium atoms forming a *3D* framework containing *1D* inorganic chains that stacked tilted along the *a*-axis. An intramolecular hydrogen bond between one of the coordinated phosphonate oxygen atom and hydroxyl group of the ligand (O4···O7 = 2.837 Å), stabilizes the metal cluster and helps propagates the *1D* chains. Adjacent chains are reinforced by two distinct intermolecular hydrogen bonds one between the amine nitrogen and hydroxyl group of the ligand (N1··· O7 = 3.008 Å), and the other between the amine nitrogen and one of the coordinated phosphonate oxygen atom (N1··· O5 = 2.689 Å) on either one side of the *1D* chains which propagate into a *3D* framework along the *bc*-plane. This crystal structure is unique from the previously discussed structure (ALEN-Ca form I) and those previously reported in the literature (Supporting Information).[32,33]

Structural description of ALEN-Zn form I, The compound $[Zn(C_4H_{11}NO_7P_2)(H_2O)]$ represents an additional crystalline phase to that originally published for the ALEN-Zn coordination complex.[34] The present structure for ALEN-Zn is isostructural to two recently published metal-phosphonate coordination complexes formed by the same ligand with either manganese or cobalt (although only the structure of ALEN-Mn is available in the Cambridge Structural Database).[23] The ALEN-Zn coordination complex is defined by the $P2_1/n$ space group and has one molecule in the asymmetric unit. The zinc atom has a strongly distorted octahedral environment with the O–Zn–O bond angles ranging from 74.74 º to 107.24 º. The Zn–O bond distances are between 1.972 and 2.353 Å. The ligand, ALEN, bridges the Zn(II) ions into an infinite single chain through four phosphonate oxygens and the hydroxyl oxygen. Inter-chain hydrogen bonds help form a *3D* network structure with channels generated along the *a*-axis. The protonated amine tails and the lattice water dwell in the channels and are held in position by intricate systems of hydrogen bonds.

Structural description of ALEN-Zn form II, The compound $[Zn_2(C_{16}H_{48}N_4O_{28}P_8)(H_2O)_2]·2H_2O$ represents an additional crystalline phase from the previously discussed phase ALEN-Zn form I. ALEN-Zn form II is a redetermination of a published structure[34] at lower temperature and present a lower error in the refinement. ALEN-Zn form II is defined by the $P2_1/n$ space group, and it's isomorphic with the structure of it Co (II)[24], Cu (II)[25], and Ni (II)[19] analogues that have been previously reported. The unit cell is composed of a centrosymmetric dinuclear coordination complex, where the metal atom coordination is octahedral. The O–Zn–O bond angles range from 82.38º to 178.59º and the Zn–O bond distances are between 2.013 and 2.156 Å. Six oxygen atoms surround the metal; two of them from a chelating BP, three are bridging the other Zn center (Zn-O-P-O-Zn) and an oxygen from the terminal water, which completes the octahedral coordination

sphere. Packing of molecules is reinforced by a rather intricate network of inter-chain hydrogen bonds among the molecular units which includes both the coordinated and the lattice water molecules.

Structural description of ALEN-Mg, The compound $[Mg_2(C_{16}H_{46}N_4O_{28}P_8(H_2O)_2]\cdot 2H_2O$ is isostructural to ALEN-Zn form II described above and to other coordination complexes with divalent metals such as Co(II)[24], Cu(II)[25], and Ni(II)[19]. The structure of ALEN-Mg is composed of a centrosymmetric dinuclear coordination complex crystallizing in the space group P2$_1$/c. The magnesium atom coordination is close to octahedral with one terminal water molecule, one terminal and two bridging ALEN ligands. The O–Mg–O bond angles range from 87.33° to 99.26°. The Mg–O bond distances are between 2.007 and 2.162 Å at the equatorial positions and between 2.007 and 2.162 Å in the axial positions. All coordinated ALEN ligands are monoanionic. The ligand, ALEN, bridges the Mg(II) ions into an infinite single chain through four phosphonate oxygens and the hydroxyl oxygen in a similar fashion as that displayed in the structure of ALEN-Zn form II. A coordination complex system of inter-chain hydrogen bonds helps form a *3D* network structure with channels generated along the *a*-axis. The protonated amine tails and the lattice water reside in the channels and are held in position by intricate systems of hydrogen bonds.
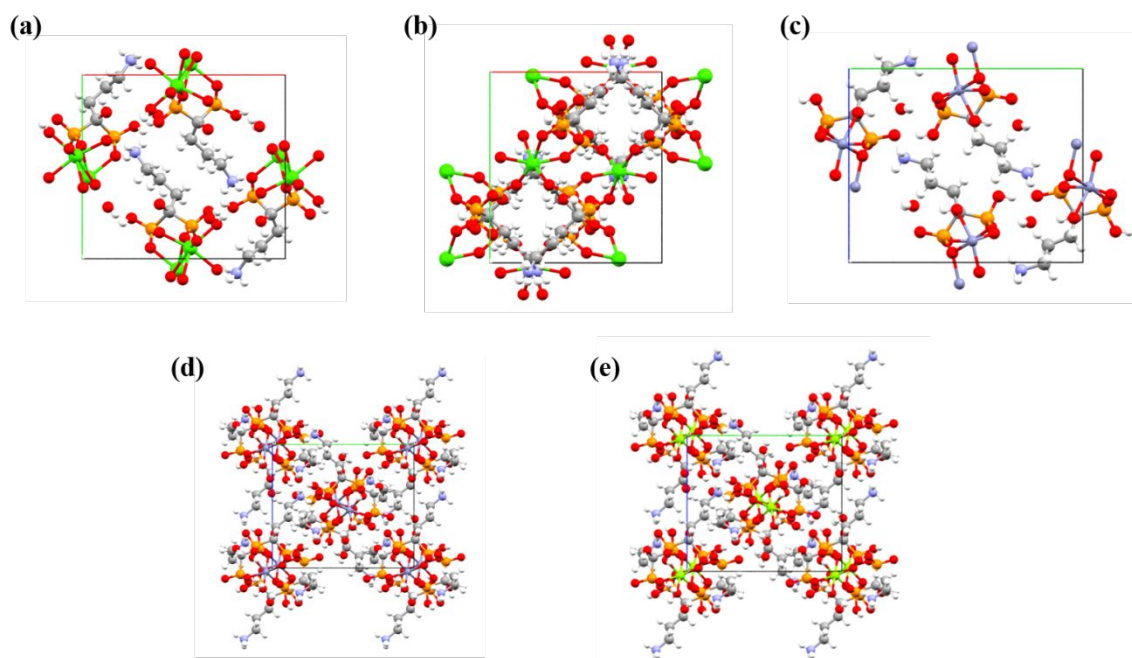

Figure 8. Packing motifs of (a) ALEN-Ca form I along the *c*-axis, (b) ALEN-Ca form II along the *c*-axis, (c) ALEN-Zn form I along the *a*-axis, (d) ALEN-Zn form II along the *a*-axis, and (e) ALEN-Mg along the *a*-axis.

Thermogravimetric analysis (TGA).

Thermal stability under N$_2$ of the isolated ALEN-based BPCCs was investigated TGA and the resulting thermographs for these materials are displayed in **Figure 9**. It was expected that the thermograph of each ALEN-based BPCCs consists of at least two mayor decomposition events one at lower temperature representing the loss of coordinated or lattice water molecules, and another at higher temperature which accounts for the thermal combustion of the organic moiety,

the BP ligand, in this case ALEN. A third decomposition event might be observed above 350 °C, due to the thermal degradation of the metal/metal oxide.
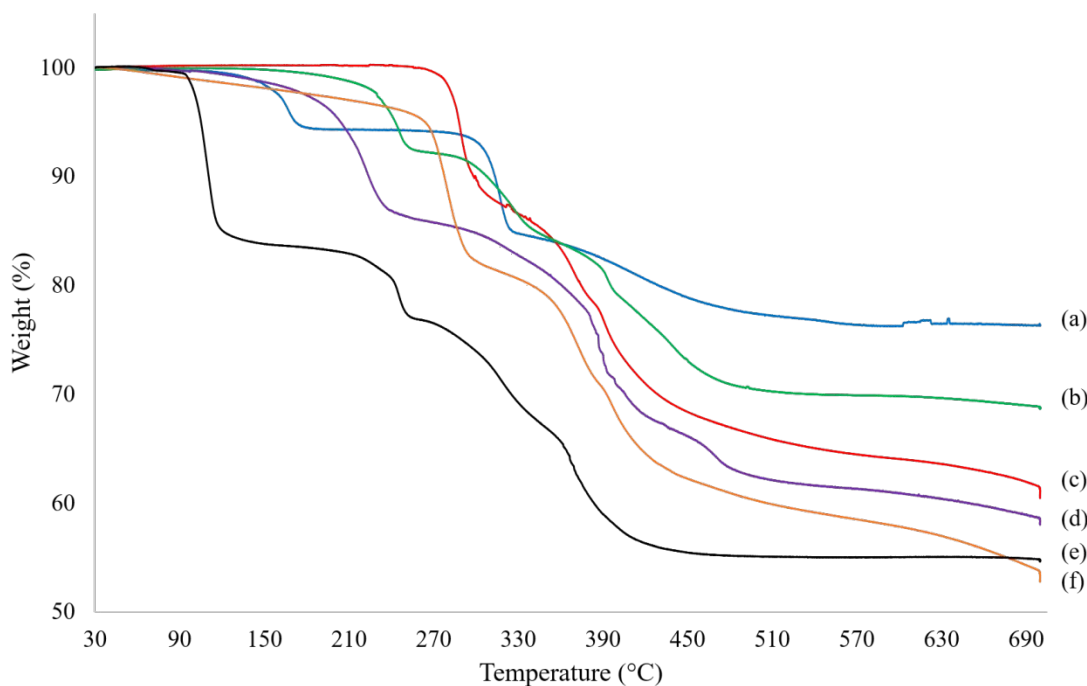
Figure 9. TGA thermographs of (a) ALEN-Ca form I, (b) ALEN-Zn form I, (c) ALEN-Ca form II, (d) ALEN-Zn form II, (e) ALEN and (f) ALEN-Mg coordination complexes. All TGA were collected with using the same temperature range between 30 – 700 °C at a heating rate of 5 °C/min under N_2.

According to the above-mentioned thermal analysis, the five ALEN-based BPCCs investigated (ALEN-Ca forms I and II, ALEN-Zn forms I and II, and ALEN-Mg) present high thermal stability than the BP (ALEN) alone. Generally, isolated ALEN-based BPCCs are stable to ~50 °C after which some of them quickly loose lattice water molecules up to 150 °C, followed by the loss of coordinated water molecules. ALEN and the ALEN-based BPCCs significantly degrade at temperatures >250 °C. Individual thermographs are available in the Supporting Information.

Dissolution profiles.

ALEN is a polyvalent strong acid with a high solubility in water.[35] Once orally administered, the dissolution of alendronate monosodium salt (*Fosamax*®) starts during deglutition.[35] This rapid dissolution affects the absorption process, lowering the dosage taken up by the skeleton (~20-50 %) and causing adverse side effects, such as esophagitis.[35] In this study, the dissolution of ALEN-based BPCCs was analyzed and compared to that of the commercially employed ALEN Sodium Tablets-USP (generic form of *Fosamax*®). Assessing the stability and equilibrium solubility of the coordination complexes in both media provides insights into the potential of ALEN-based BPCCs to sustain blood plasma concentrations for ALEN. Additionally, tumor metastases and bone resorption are closely associated with an acidic microenvironment,[36,37,38] which may alter substantially the structure of these materials, promoting their degradation at the metastatic site.

Direct quantification of ALEN was hampered by the lack of a detectable chromophore.

Therefore, the formation of an ALEN-Cu complex was employed as a suitable method of quantification for the released content from the ALEN-based BPCCs as previously employed for ALEN and risedronic acid.[22,39] Compared to the ALEN-based BPCCs, the ALEN-Cu complex and other BP-Cu salts tend to have higher solubility at lower to neutral pH.[22] In this study, quantification of the drug release in acidic (FaSSGF, pH = 1.60) and neutral (PBS, pH = 7.40) media was conducted, permitting the optimum conditions for promoting the formation of the UV active ALEN-Cu complex and avoiding its precipitation.

The administered dosage of ALEN in tablets is 70 mg, which correspond to the initial weight for the ALEN-based BPCCs and the commercial generic form of ALEN used for the dissolution testing.[35] To verify the maximum amount of ALEN released, a complete dissolution profile was obtained in FaSSGF. The dissolution profile (**Figure 10a**) showed that ALEN reaches the maximum release of the drug (100%) faster (10 sec) compared to the ALEN-based BPCCs. The generic tablets achieved a 100% release in 25 sec. All ALEN-based BPCCs presented lower equilibrium solubility and dissolution in FaSSGF.

For the simulated drug release in physiological pH conditions, dissolution was conducted in PBS. After comparing the complete dissolution profile in this media for each coordination complex (**Figure 10b**), results demonstrate that the generic tablets have a higher dissolution rate, reaching the maximum release of the ALEN content (80%) in 25 sec. The dissolution of ALEN showed a slower release but reached a similar amount of dissolved drug as the generic tablets (~80 %) in 10 min. The BPCCs also showed a lower dissolution and equilibrium solubility compared to the tablets and the reagent in this media.

Based on these results, we decided to perform further studies with ALEN-Ca form II, which presented lower dissolution and equilibrium solubility in PBS (pH = 7.40) but higher dissolution and solubility in FaSSGF (pH = 1.60). These characteristics are desirable because it may allow nanoparticles of this material to circulate longer allowing them to reach the target site (bone microenvironment). Once there, the material might be able to degrade due to the increased acidic microenvironment at the metastatic site.[36,37,38] These results provide insights of the potential of these coordination complexes to release the BP content by their degradation in a selective manner.
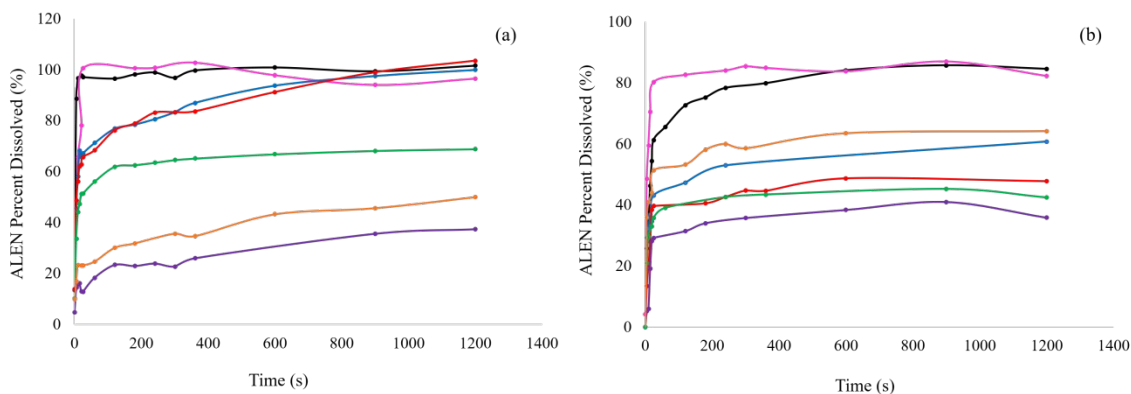
Figure 10. Complete dissolution profile for ALEN (black), Alendronate Sodium (Fosamax®) generic tablets (pink), ALEN-Ca form I (blue), ALEN-Ca form II (red), ALEN-Zn form I (green), ALEN-Zn form II (purple) and ALEN-Mg (orange) in (a) FaSSGF and (b) PBS.
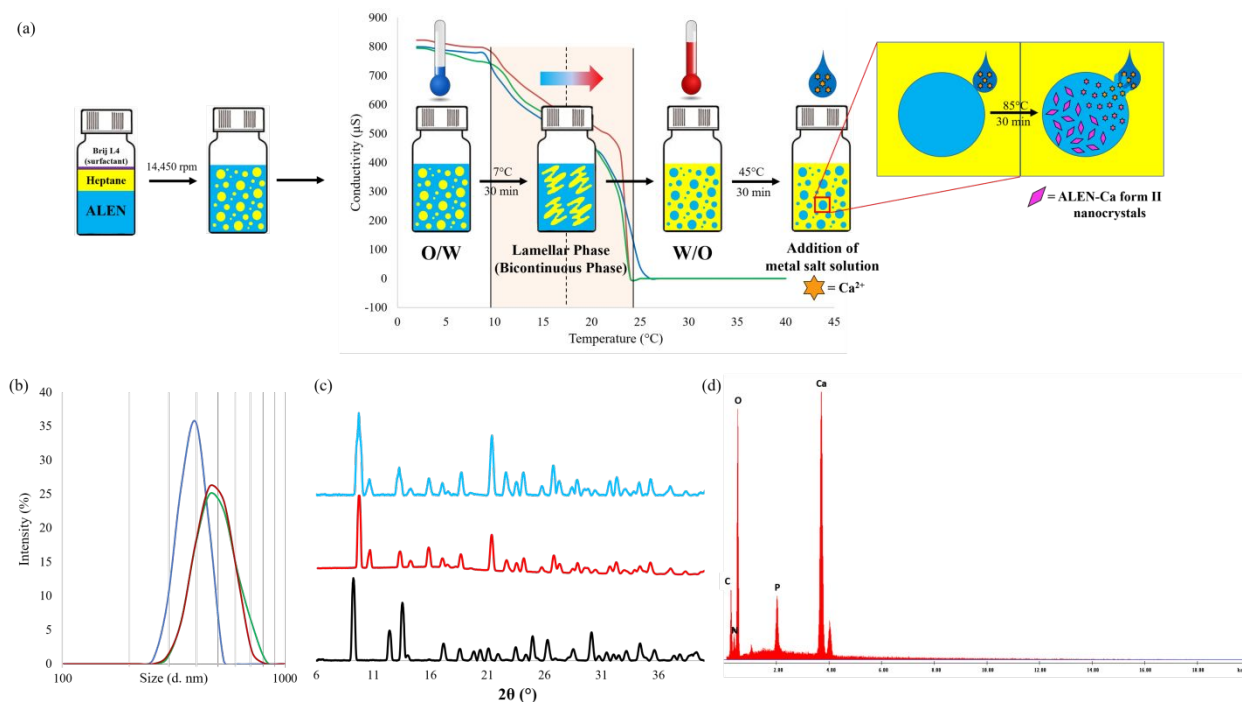
Phase inversion temperature (PIT)-nano-emulsion synthesis of nano-Ca@ALEN form II.

In order to reduce the particle size, a PIT-nano-emulsion method was employed during the

synthesis of a selected ALEN-based BPCC, specifically ALEN-Ca form II. Selection of ALEN-Ca form II was based on its promising porous crystal structure, higher thermal stability, and selective degradation (PBS versus FaSSGF). The PIT temperature was determined by measuring the conductivity of an aqueous emulsion containing ALEN in heptane and a surfactant. After homogenizing the emulsions, conductivity measurements started at 2°C with the oil-in-water (O/W) system reporting an average value of 808 µS at the starting point. As the emulsion is heated (1°C/min), a phase inversion occurs from O/W (conductive) micro-emulsion to water in oil (W/O, not conductive) nano-emulsion. Once the temperature reached 24°C, the conductivity dropped, reporting average values of ~0.019 µS.

Once the PIT was identified, it was used to perform the synthesis of nano-Ca@ALEN form II (**Figure 11a**). After having the ligand solution entrapped in the nanospheres suspended in the oil phase of the emulsion, addition of the metal promoted the formation of the nano-Ca@ALEN form II nanoparticles. Once the reaction was completed, the aqueous supernatant was analyzed using DLS. Results demonstrate average particle size distribution values of 383.9, 482.5 and 495.3 nanometers for three replicate syntheses (**Figure 11b** and Supporting Information). Polydispersity index (PDI) average values of 0.870, 0.631 and 0.645 were obtained. According to the PDI values, the nano-Ca@ALEN form II nanoparticles measured were moderately monodispersive. Results demonstrate that this method reduces the particle size of ALEN-Ca form II from a micron-range (~60 µm) to a nano-range (380-495 d.nm), possibly by reducing the volume available for the metal complexation (precipitation) to occur. PXRD analysis was performed on a micron-sized agglomerate (Supporting Information) of the nanocrystals resulting from the PIT-nanoemulsion. PXRD analysis confirms that the crystal phase of the nano-Ca@ALEN form II nanoparticles is isostructural to that of ALEN-Ca form II bulk crystals (**Figure 11c**). The EDS spectra of nano-Ca@ALEN form II nanoparticles exhibit characteristic signals of the metal and other elements, which are present in this BPCC and resembles the EDS spectra of the bulk material (**Figure 11d**). This data corroborates the composition of the nano-Ca@ALEN form II in the nanoparticles synthesized by the proposed method based on the elemental analysis. It is worth mentioning that no toxic organic solvents were required (heptane is Class 3) to develop these materials at both the bulk and nanoscale, which means that the procedure could be well adapted for large-scale biomedical manufacturing and applications.

Figure 11. (a) Schematic diagram of the PIT-nano-emulsion synthesis of nano-Ca@ALEN form II, showing the phase inversion at a temperature of approximately ~ 17°C (dashed line). Phase inversion starts at a temperature of ~9°C and ends at a temperature of ~24°C (light orange region). (b) Dynamic light scattering (DLS) spectra showing average size distribution (380-495 d.nm) of nano-Ca@ALEN form II nanoparticles. (c) PXRD overlay of ALEN (black), ALEN-Ca form II bulk crystals (red), and nano-Ca@ALEN form II agglomerated nanocrystals (light blue). (d) Representative energy dispersive spectra (EDS) for the isolated product of the PIT-micro-emulsion synthesis between ALEN and bioactive metal calcium (Ca^{2+}).

Cytotoxicity assay of ALEN, ALEN-Ca form II (bulk crystals) and nano-Ca@ALEN form II (nanocrystals).

Dose response curves for ALEN and ALEN-Ca form II (bulk crystals) were performed in breast cancer cell line MDA-MB-231. After 24, 48 and 72 h the potency of ALEN or ALEN-Ca form II (bulk crystals) treatment was measured using AlamarBlue® cell viability assay. After 24 h both, ALEN and ALEN form II (bulk crystals), did not showed a significant cytotoxicity effect in MDA-MB-231 with $IC_{50} > 100$ µM (Supporting Information). However, after 48 h, an increased in potency for both ALEN and ALEN-Ca form II (bulk crystals) was observed. The viability of MDA-MB-231 cells treated with ALEN and ALEN-Ca form II (bulk crystals) decreased approximately by 50.63 % and 57.94 %, with an $IC_{50} > 100$ µM, respectively (Supporting Information). Finally, after 72 h of treatment an IC_{50} of 15.0 ± 0.4 and 32 ± 1 µM for ALEN and ALEN-Ca form II (bulk crystals) was obtained, respectively (Supporting Information). ALEN has shown cytotoxicity effects through the inhibition of proliferation in other cancer cell lines in a dose and time dependent manner. Results obtained within this study are in accordance with those previously reported in literature.[40,41]
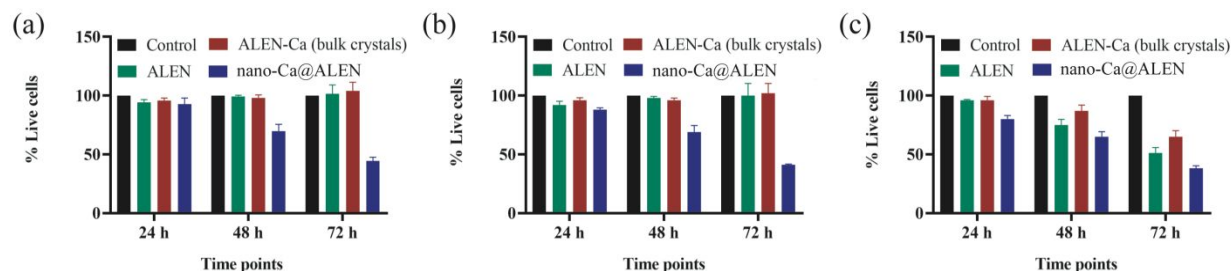
Figure 12. Relative cell viability (%) of MDA-MD-231 cell line (control, black) treated with ALEN, ALEN-Ca form II (bulk, red) and nano-Ca@ALEN form II (nanocrystals, blue) in concentrations of (a) 7.5 μM (b) 15 μM, and (c) 30 μM at 24, 48 and 72 h of treatment.

The relative cell live viability was determined in the following concentrations; 7.5, 15 and 30 μM for ALEN, ALEN-Ca form II (bulk crystals), and nano-Ca@ALEN form II (nanocrystals) after 24, 48, and 72 h of treatment (**Figure 12a**). The results showed that nano-Ca@ALEN form II nanocrystals present cytotoxicity effects against the MDA-MB-231 cell line. Particularly, an inhibition of cell growth was observed after 24 h of treatment, even at the lowest concentration (7.5 μM). **Figure 12a** shows that at 72 h of treatment in a concentration of 7.5 μM, the cell viability decreases from 100 % to 46 ± 11 % for nano-Ca@ALEN form II nanocrystals, while for ALEN and ALEN-Ca form II (bulk crystals) no significant cell death is observed.

Conclusions.

Herein, we have described the hydrothermal reaction and the structural characterization of a series of ALEN-based BPCCs constructed by employing clinically utilized BP, ALEN, as ligand and three biologically relevant metals (Ca^{2+}, Zn^{2+} and Mg^{2+}). An unprecedented number of ALEN-based BPCCs were obtained and structurally characterized to provide further insights into the structural motifs observed in these types of materials. These compounds have been obtained as single phases and exhibit high to moderate thermal stability. Dissolution test results provided insights of their structural stability in simulated physiological conditions (FaSSGF and PBS). Most of the studied ALEN-based BPCCs remained coordinated, thus presented higher stability and lower equilibrium solubility in both media. This suggests that the incorporation of ALEN as a constituent of the CC, lead to the formation of a system that can potentially promote higher blood plasma concentrations of ALEN. The PIT-nano emulsion synthesis method provided a soft confinement approach to reduce the particle size of one of the ALEN-based BPCCs, ALEN-Ca form II significantly. PIT-nano emulsion synthesis could be easily translated to other BPCCs. A size decrease in the particle size of the BPCCs presents several advantages towards advancing the therapeutic applications of these coordination complexes, potentiating these materials for the treatment and prevention of OM. Furthermore, the cytotoxicity of ALEN and ALEN-Ca form II (bulk crystals) and nano-Ca@ALEN form II (nanocrystals) was investigated to determine if the size and chemical nature of this BPCC could enhance the cytotoxicity of ALEN against the MDA-MB-231 cell line. Results demonstrate that after 72 h of treatment, the cell viability decreases to 46 ± 11 % for nano-Ca@ALEN form II nanocrystals, while for ALEN and ALEN-Ca form II (bulk crystals) no significant cell death was observed. These important outcomes provide the integration and expansion of the molecular design principles concerning drug delivery systems based on BPCCs that can be used to treat and prevent OM and other bone-related diseases.

Supporting Information. Detailed experimental procedures for the hydrothermal synthesis,

additional Raman spectra, powder X-ray diffractograms, SEM images, EDS spectra, TGA thermographs, crystallographic parameters, CIF files, ORTEPs, calibration curves, absorption spectra, dissolution profiles, DLS spectra can be obtained free of charge via the Internet at http://pubs.rsc.org.

Corresponding Author.
E-mail address: vilmali.lopez@upr.edu

**Conflicts of Interest.**
There are no conflicts of interest to declare.

References.
(1) Ferlay, J.; Colombet, M.; Soerjomataram, I.; Mathers, C.; Parkin, D. M.; Piñeros, M.; Znaor, A.; Bray, F. Estimating the Global Cancer Incidence and Mortality in 2018: GLOBOCAN Sources and Methods. *International Journal of Cancer*. Wiley-Liss Inc. April 15, 2019, pp 1941–1953. https://doi.org/10.1002/ijc.31937.
(2) Croset, M.; Clézardin, P. MicroRNA-Mediated Regulation of Bone Metastasis Formation: From Primary Tumors to Skeleton. In *Bone Cancer: Primary Bone Cancers and Bone Metastases: Second Edition*; Elsevier Inc., 2014; pp 479–489. https://doi.org/10.1016/B978-0-12-416721-6.00041-8.
(3) Welsh, J. E. Animal Models for Studying Prevention and Treatment of Breast Cancer. In *Animal Models for the Study of Human Disease*; Elsevier Inc., 2013; pp 997–1018. https://doi.org/10.1016/B978-0-12-415894-8.00040-3.
(4) Perez-Garcia, J.; Muñoz-Couselo, E.; Cortes, J. Bone Metastases: Causes, Consequences and Therapeutic Opportunities. In *European Journal of Cancer, Supplement*; 2013; Vol. 11, pp 254–256. https://doi.org/10.1016/j.ejcsup.2013.07.035.
(5) Mundy, G. R. Metastasis to Bone: Causes, Consequences and Therapeutic Opportunities. *Nature Reviews Cancer*. August 2002, pp 584–593. https://doi.org/10.1038/nrc867.
(6) Diba, M.; Camargo, W. A.; Zinkevich, T.; Grünewald, A.; Detsch, R.; Kabiri, Y.; Kentgens, A. P. M.; Boccaccini, A. R.; Van Den Beucken, J. J. J. P.; Leeuwenburgh, S. C. G. Hybrid Particles Derived from Alendronate and Bioactive Glass for Treatment of Osteoporotic Bone Defects. *J. Mater. Chem. B* **2019**, *7* (5), 796–808. https://doi.org/10.1039/c8tb03062f.

(7)   Paolino, D.; Licciardi, M.; Celia, C.; Giammona, G.; Fresta, M.; Cavallaro, G. Bisphosphonate-Polyaspartamide Conjugates as Bone Targeted Drug Delivery Systems. *J. Mater. Chem. B* **2015**, *3* (2), 250–259. https://doi.org/10.1039/c4tb00955j.

(8)   Guenin, E.; Ledoux, D.; Oudar, O.; Lecouvey, M.; Kraemer, M. Structure-Activity Relationships of a New Class of Aromatic Bisphosphonates That Inhibit Tumor Cell Proliferation in Vitro. *Anticancer Res* **2005**, *25* (2A), 1139–1145.

(9)   Giger, E. V.; Castagner, B.; Leroux, J. C. Biomedical Applications of Bisphosphonates. *J. Control. Release* **2013**, *167* (2), 175–188. https://doi.org/10.1016/j.jconrel.2013.01.032.

(10)   Heymann, D.; Ory, B.; Gouin, F.; Green, J. R.; Rédini, F. Bisphosphonates: New Therapeutic Agents for the Treatment of Bone Tumors. *Trends in Molecular Medicine*. July 1, 2004, pp 337–343. https://doi.org/10.1016/j.molmed.2004.05.007.

(11)   Cells, C.; Bone, T. O.; Vitro, I. N. No Title. **1995**, *17* (6), 1995.

(12)   Liu, D.; He, C.; Poon, C.; Lin, W. Theranostic Nanoscale Coordination Polymers for Magnetic Resonance Imaging and Bisphosphonate Delivery. *J. Mater. Chem. B* **2014**, *2* (46), 8249–8255. https://doi.org/10.1039/c4tb00751d.

(13)   Clezardin, P.; Ebetino, F. H.; Fournier, P. G. Bisphosphonates and Cancer-Induced Bone Disease: Beyond Their Antiresorptive Activity. *J. Cancer Res.* **2005**, *65* (12), 4971–4974.

(14)   Alasmari, A.; Lin, S. C.; Dibart, S.; Salih, E. Bone Microenvironment-Mediated Resistance of Cancer Cells to Bisphosphonates and Impact on Bone Osteocytes/Stem Cells. *Clin. Exp. Metastasis* **2016**, *33* (6), 563–588. https://doi.org/10.1007/s10585-016-9798-6.

(15)   Article, R. <Bisphosphonates - a Review of Their PK Properties (Lin).Pdf>. **1996**, *3282* (2), 75–85.

(16)   Khosla, S.; Bilezikian, J. P.; Dempster, D. W.; Lewiecki, E. M.; Miller, P. D.; Neer, R. M.; Recker, R. R.; Shane, E.; Shoback, D.; Potts, J. T. Benefits and Risks of Bisphosphonate Therapy for Osteoporosis. *Journal of Clinical Endocrinology and Metabolism*. July 2012, pp 2272–2282. https://doi.org/10.1210/jc.2012-1027.

(17)   Saad, A.; Rousseau, G.; El Moll, H.; Oms, O.; Mialane, P.; Marrot, J.; Parent, L.; Mbomekallé, I. M.; Dessapt, R.; Dolbecq, A. Molybdenum Bisphosphonates with Cr(III) or Mn(III) Ions. *J. Clust. Sci.* **2014**, *25* (3), 795–809. https://doi.org/10.1007/s10876-013-0655-3.

(18)   Deacon, G. B.; Greenhill, N. B.; Junk, P. C.; Wiecko, M. Synthesis and Crystal Structure of Lithium Alendronate. *J. Coord. Chem.* **2011**, *64* (1), 179–185. https://doi.org/10.1080/00958972.2010.538389.

(19)   Sikorska, M.; Gazda, M.; Chojnacki, J. Nickel Alendronate. *Acta Crystallogr. Sect. E Struct. Reports Online* **2012**, *68* (6). https://doi.org/10.1107/S1600536812022532.

(20)   Hu, J.; Zhao, J.; Hou, H.; Fan, Y. Syntheses, Structures and Fluorescence Studies of Two New Cadmium(II) Pyridyl-Diphosphonates. *Inorg. Chem. Commun.* **2008**, *11* (10), 1110–1112. https://doi.org/10.1016/j.inoche.2008.06.013.

(21)   Demoro, B.; Caruso, F.; Rossi, M.; Benítez, D.; Gonzalez, M.; Cerecetto, H.; Parajón-Costa, B.; Castiglioni, J.; Galizzi, M.; Docampo, R.; et al. Risedronate Metal Complexes Potentially Active against Chagas Disease. *J. Inorg. Biochem.* **2010**, *104* (12), 1252–1258. https://doi.org/10.1016/j.jinorgbio.2010.08.004.

(22)   Ostovic, D.; Stelmach, C.; Hulshizer, B. Formation of a Chromophoric Complex Between Alendronate and Copper(II) Ions. *Pharm. Res.* **1993**, *10* (3), 470–472.

(23)   Zhang, Z. C.; Bao, S. S.; Zheng, L. M. Ladder-like Metal Diphosphonates Exhibiting Field-Induced Magnetic Transitions. *Inorg. Chem. Commun.* **2007**, *10* (9), 1063–1066.

https://doi.org/10.1016/j.inoche.2007.05.028.

(24)   Man, S. P.; Motevalli, M.; Gardiner, S.; Sullivan, A.; Wilson, J. Structural Studies on New Metal Derivatives of Osteoporosis Therapeutic Aminohydroxyalkylidenebisphosphonic Acids with C4 and C6 Aminoalkyl Chains. *Polyhedron* **2006**, *25* (4), 1017–1032. https://doi.org/10.1016/j.poly.2005.12.009.

(25)   Biot, C.; Castro, W.; Botté, C. Y.; Navarro, M. The Therapeutic Potential of Metal-Based Antimalarial Agents: Implications for the Mechanism of Action. *Dalton Transactions*. June 7, 2012, pp 6335–6349. https://doi.org/10.1039/c2dt12247b.

(26)   Kennel, K. A.; Drake, M. T. Adverse Effects of Bisphosphonates: Implications for Osteoporosis Management. *Mayo Clinic Proceedings*. Elsevier Ltd 2009, pp 632–638. https://doi.org/10.4065/84.7.632.

(27)   Castiglioni, S.; Cazzaniga, A.; Albisetti, W.; Maier, J. A. M. Magnesium and Osteoporosis: Current State of Knowledge and Future Research Directions. *Nutrients*. MDPI AG 2013, pp 3022–3033. https://doi.org/10.3390/nu5083022.

(28)   Yamaguchi, M. Role of Nutritional Zinc in the Prevention of Osteoporosis. *Molecular and Cellular Biochemistry*. May 2010, pp 241–254. https://doi.org/10.1007/s11010-009-0358-0.

(29)   Cukrowski, I.; Popović, L.; Barnard, W.; Paul, S. O.; van Rooyen, P. H.; Liles, D. C. Modeling and Spectroscopic Studies of Bisphosphonate-Bone Interactions. The Raman, NMR and Crystallographic Investigations of Ca-HEDP Complexes. *Bone* **2007**, *41* (4), 668–678. https://doi.org/10.1016/j.bone.2007.05.008.

(30)   Au, K. M.; Satterlee, A.; Min, Y.; Tian, X.; Kim, Y. S.; Caster, J. M.; Zhang, L.; Zhang, T.; Huang, L.; Wang, A. Z. Folate-Targeted PH-Responsive Calcium Zoledronate Nanoscale Metal-Organic Frameworks: Turning a Bone Antiresorptive Agent into an Anticancer Therapeutic. *Biomaterials* **2016**, *82*, 178–193. https://doi.org/10.1016/j.biomaterials.2015.12.018.

(31)   Bell, R. V.; Rochford, L. A.; De Rosales, R. T. M.; Stevens, M.; Weaver, J. V. M.; Bon, S. A. F. Fabrication of Calcium Phosphate Microcapsules Using Emulsion Droplets Stabilized with Branched Copolymers as Templates. *J. Mater. Chem. B* **2015**, *3* (27), 5544–5552. https://doi.org/10.1039/c5tb00893j.

(32)   Fernández, D.; Vega, D.; Goeta, A. Alendronate Zwitterions Bind to Calcium Cations Arranged in Columns. *Acta Crystallogr. Sect. C Cryst. Struct. Commun.* **2003**, *59* (12). https://doi.org/10.1107/S0108270103025599.

(33)   Alvarez, E.; Marquez, A. G.; Devic, T.; Steunou, N.; Serre, C.; Bonhomme, C.; Gervais, C.; Izquierdo-Barba, I.; Vallet-Regi, M.; Laurencin, D.; et al. A Biocompatible Calcium Bisphosphonate Coordination Polymer: Towards a Metal-Linker Synergistic Therapeutic Effect? *CrystEngComm* **2013**, *15* (46), 9899–9905. https://doi.org/10.1039/c3ce41346b.

(34)   Dufau, C.; Benramdane, M.; Leroux, Y.; Manouni, D. El; Neuman, A.; Prangé, T.; Silvestre, J.-P.; Gillier, H. Étude De La Complexation Du Cadmium Et Du Zinc Avec L'Alendronate (Acide 4-Amino-1-Hydroxybutylidène-1'1-Bisphosphonique). *Phosphorus, Sulfur Silicon Relat. Elem.* **1995**, *107* (1), 145–159. https://doi.org/10.1080/10426509508027930.

(35)   Lamprecht, G. In Vitro Determination of Th Release of Alendronic Acid from Alendronate Tablets of Different Brands during Deglutition. *J. Pharm. Sci.* **2009**, *98* (10), 3575–3581.

(36)   Kato, Y.; Ozawa, S.; Miyamoto, C.; Maehata, Y.; Suzuki, A.; Maeda, T.; Baba, Y. Acidic Extracellular Microenvironment and Cancer. *Cancer Cell International*. September 3, 2013. https://doi.org/10.1186/1475-2867-13-89.

(37) Coleman, R.; Body, J. J.; Aapro, M.; Hadji, P.; Herrstedt, J. Bone Health in Cancer Patients: ESMO Clinical Practice Guidelines. *Ann. Oncol.* **2014**, *25*, 124–137. https://doi.org/10.1093/annonc/mdu103.

(38) Tsuzuki, S.; Park, S. H.; Eber, M. R.; Peters, C. M.; Shiozawa, Y. Skeletal Complications in Cancer Patients with Bone Metastases. *International Journal of Urology*. Blackwell Publishing October 1, 2016, pp 825–832. https://doi.org/10.1111/iju.13170.

(39) Walash, M. I.; Metwally, M. E. S.; Eid, M.; El-Shaheny, R. N. Spectrophotometric Determination of Risedronate in Pharmaceutical Formulations via Compkex Formation with Cu (II) Ions: Application to Content Uniformity Testing. *Int. J. Biomed. Sci.* **2088**, *4* (4), 303–309.

(40) Ilyas, A.; Hashim, Z.; Naeem, N.; Haneef, K.; Zarina, S. The Effect of Alendronate on Proteome of Hepatocellular Carcinoma Cell Lines. *Int. J. Proteomics* **2014**, *2014*, 1–9. https://doi.org/10.1155/2014/532953.

(41) Jiang, P.; Zhang, P.; Mukthavaram, R.; Nomura, N.; Pingle, S. C.; Teng, D.; Chien, S.; Guo, F.; Kesari, S. Anti-Cancer Effects of Nitrogen-Containing Bisphosphonates on Human Cancer Cells. *Oncotarget* **2016**, *7* (36). https://doi.org/10.18632/oncotarget.10773.
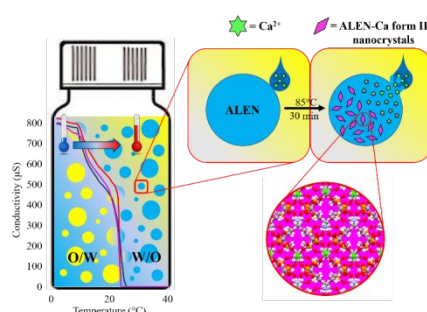
The phase-inversion hydrothermal synthesis of alendronate and Ca(II) promotes the formation a coordination complex which solid-state, stability, particle size and cytotoxicity were assessed and optimized to potentiate its biomedical applications.